Zhang *et al.*
EURASIP Journal on Advances in Signal Processing (2023) 2023:23
https://doi.org/10.1186/s13634-023-00985-5

EURASIP Journal on Advances in Signal Processing

RESEARCH Open Access

Application of IMMF–IHHT algorithm to suppressing random interference of geomagnetic sensors

Ping-an Zhang, Min Gao*, Wei Wang, Yi Wang and Xu-jun Su

*Correspondence: gaimin6310@163.com

Shijiazhuang Campus of Army Engineering University, Shijiazhuang, China

Abstract

Aiming at the problem that the geomagnetic sensor is vulnerable to external interference in the navigation process, this paper analyzes the frequency distribution range of geomagnetic signal and the noise characteristics in geomagnetic signal and proposes an improved morphological filtering and Hilbert–Huang transform (IMMF–IHHT) algorithm to extract and recognize the features of geomagnetic measurement signal. To avoid frequency aliasing and distortion caused by empirical mode decomposition, an improved morphological filtering algorithm based on mean constraint is used to preprocess the measured signal. The Hilbert spectrum of the decomposed signal is solved, the signal components are discriminated by the similarity criterion, and the signal components in line with the frequency range of the geomagnetic signal are extracted and processed to reconstruct the geomagnetic measurement signal. Simulation and experiments show that the signal-to-noise ratio and root-mean-square error of IMMF–IHHT combination algorithm are better than MF-HHT combination algorithm and IHHT algorithm. This algorithm has good signal feature extraction and recognition ability.

Keywords: Geomagnetic sensor, Improved morphological filtering (IMMF), Improved Hilbert–Huang transform (IHHT), Feature extraction and recognition, Similarity criterion

1 Introduction

In the field of geomagnetic navigation, the fixed magnetic field, induced magnetic field and various random magnetic fields in the environment of the navigation carrier will interfere with the measurement of geomagnetic field [1–3]. Therefore, effectively eliminating the interfering magnetic field in the magnetic measurement environment is the key problem to improve the accuracy of geomagnetic navigation [4]. In particular, there is little research on the processing method and theory of random interference magnetic field. In geomagnetic measurement signals, random interference signals have the characteristics of wide frequency band and strong randomness, which is the primary problem to improve the accuracy of geomagnetic navigation. Therefore, this paper analyzes the random interference magnetic field in the magnetic measurement environment and studies the methods to effectively reduce the influence of random interference magnetic field.

The sources of random interference magnetic field in the magnetic measurement environment include the high-frequency interference caused by the current change in the electronic equipment of the carrier itself, the electromagnetic interference in the environmental magnetic field and the noise generated by the sensor in the measurement process, which will affect the output of the geomagnetic sensor [5–7]. At present, the methods of magnetic field compensation for random interference of magnetic sensors include wavelet threshold denoising algorithm, particle filter, morphological filter (MF) [8], adaptive median filter and Hilbert–Huang transform based on classical modal decomposition [4]. Shi [9] compensated the random interference of magnetic sensors by studying the wavelet transform algorithm based on improved threshold and MLS-SVR [10] inversion based on particle swarm optimization, which was applied to the defect detection of oil and gas pipelines; Shan [11] proposed a denoising algorithm using wavelet transform to eliminate the magnetic anomaly signal in the measurement process; Xie fan [12] used mathematical morphological filtering to suppress pulse interference and reduce the noise interference of the sensor according to the interference signal characteristics of the magnetic sensor; and Huang [13] proposed an adaptive data analysis method using Hilbert–Huang transform method for classical modal decomposition, which is applied to geomagnetic measurement of magnetic sensors. Single filter has its own limitations, such as the long running time of wavelet algorithm and particle swarm optimization algorithm; when MF is used to deal with the noise in the signal, the open operation and close operation process in morphological filtering are limited by the length of structural elements, so it is impossible to process the whole signal; and empirical mode decomposition (EMD) in HHT algorithm cannot decompose the aliasing components in geomagnetic signal. At the same time, it has poor processing effect for strong noise, which is easy to cause signal distortion after reconstruction and so on.

In view of the limitation of single filtering, many scholars combine two or more filtering methods for signal noise reduction. Li Ji [14] combined morphological filtering and Hilbert–Huang transform. Morphological filtering was used to process the data to eliminate the influence of instantaneous strong pulse firstly, and then, Hilbert–Huang transform was used to decompose the signal and identify the high-frequency noise component, which can effectively suppress the interference noise of magnetic sensor. Based on Li Ji's research method, Diao Yun-yun [15] introduced autocorrelation function to verify that the high-order components above order 6 contain effective geomagnetic signal cutoff frequency, identify the effective geomagnetic signal in the medium and high-frequency components of IMF and calculate the root-mean-square error (RMSE) between the final result and the fast Fourier transform result, proving the superiority of morphological filtering and HHT combined filtering. Zhai [16] adopted the improved empirical mode decomposition for geomagnetic measurement signals, designed normalized least mean square (NLMS) filter and morphological filter to remove the noise in the mixed intrinsic mode function (IMF), adaptively adjusted the filtering parameters according to the noise level of different IMF components, reconstructed the IMF and residual after noise reduction and obtained the filtered signal. Zhou [17] used the combined filtering algorithm of adaptive median filter and HHT algorithm for magnetic sensor signal processing and proposed a similarity criterion based on IMF processing. To distinguish the geomagnetic signal and high-frequency signal in IMF, the high-frequency signal in IMF is eliminated through adaptive median filter, and the

processed signal is obtained by reconstructing between each IMF and residual. The experimental results show that the adaptive median filter and the improved HHT combined filter algorithm greatly enhance the calibration performance, and the error is reduced by more than 50% compared with the results of other methods. Therefore, according to the characteristics of geomagnetic signal, this paper combines the improved morphological filtering algorithm and HHT algorithm to extract and recognize the characteristics of geomagnetic measurement signal.

Aiming at the problem that the open close operation in morphological filtering will make the calculation result smaller and the close open operation will make the calculation result larger, this paper introduces the restriction of the length of structural elements corresponding to the mean value of the original signal to obtain the preprocessed geomagnetic measurement signal. Then, the preprocessed signal is decomposed by EMD, the Hilbert spectrum is solved, and the similarity criterion is introduced to judge the IMF component. The similarity criterion uses the instantaneous frequency of each IMF component in the Hilbert spectrum, compares the distribution range of instantaneous frequency with the frequency distribution range of geomagnetic signal, classifies the IMF components, completes the processing of IMF components, respectively, and reconstructs the processed IMF components and residuals. In this paper, the improved morphological filtering and HHT algorithm are combined to realize the feature extraction and recognition of geomagnetic sensor signal.

The rest of this paper is organized as follows. The second part mainly expounds the theory of improved morphological filtering algorithm and HHT algorithm in detail. In the third part, the IMMF–IHHT algorithm is simulated and compared. In the fourth part, the experiment of simulated vibration turntable is carried out. Finally, the fifth and sixth parts are discussed and summarized.

2 Theoretical analysis

2.1 IMMF theory

Mathematical morphological filtering was founded by French mathematicians Matheron and Serra in the 1960s. It is a method closely related to mathematical theory and engineering practice, which can be used for nonlinear signal (image) processing. Using mathematical morphological transformation, namely corrosion, expansion, morphological opening and morphological closing operations, the complex signal can be decomposed into various parts with physical significance, stripped from the background and maintained its main characteristics. Basic mathematical morphological operation process is:

Let $f(n)$ and $g(m)$ be discrete functions defined in $n=1,2,\sim n$ and $m=1,2,\sim M$ (M usually takes an odd number), respectively, where $f(n)$ is the original signal containing noise, $g(m)$ is the structural element, $n>>m$. Then, the corrosion and expansion calculations of with respect to g are:

$$f\Theta g(n) = \min_{m=1,2,\cdots,M} [f(n+m) - g(m)] \tag{1}$$

$$f \oplus g(n) = \max_{m=1,2,\cdots,M} [f(n-m) + g(m)] \tag{2}$$

In Eqs. 1 and 2,Θ and $\oplus$ are defined as corrosion and expansion operations, respectively. The open and close operations of f on g are:

$$\begin{cases} (f \circ g)(n) = (f \Theta g \oplus g)(n) \\ (f \bullet g)(n) = (f \oplus g \Theta g)(n) \end{cases} \tag{3}$$

In the above formula, $\circ$ and $\bullet$ are defined as card operation and closed operation, respectively. The open operation and close operation in morphological filtering have different effects on signal processing. The open operation can eliminate the positive peak, and the close operation can eliminate the negative peak. To eliminate the influence of positive and negative peaks at the same time, the same structural elements are usually used to construct open–close and close–open morphological filters in different sequential cascading modes, which are expressed as:

$$\begin{cases} H_{\mathrm{oc}}(n) = (f \circ g \bullet g)(n) \\ H_{\mathrm{co}}(n) = (f \bullet g \circ g)(n) \end{cases} \tag{4}$$

Morphological open–close and close–open filters have all the characteristics of open operation and close operation. Open operation will lead to small output of open–close filter, and closed operation will lead to large output of close–open filter. Therefore, the general morphological filter takes the average value of open–close and close–open filter. This algorithm defaults to open–close and close–open filters. This algorithm defaults to open–close and close–open filters. The offset of each sampling point is the same, or the difference is small, which reduces the performance of the filter. To improve the noise reduction performance of the filter, this paper constructs an open–close and close–open combined filter by cascading two filters and introducing the constraint parameter H. The constraint conditions are as follows:

$$H(n) = \underset{m=1,2,\cdots,M}{\mathrm{mean}} \left[f\left(n - \frac{M-1}{2}\right), \ldots, f(n), \ldots, f\left(n + \frac{M-1}{2}\right) \right] \tag{5}$$

The calculation method of filtered signal $f^*(n)$ can be divided into three judgment methods. When the results of the closed-open filter and the open–closed filter are the same, both of them can be regarded as the final results; when the results of the closed-open filter and the open–closed filter are different, they can be divided into two types. If one of the two filters is equal to the average value, the average value shall be selected as the final result; otherwise, the average value of the three filters $(H(n), H_{\mathrm{co}}(n), H_{\mathrm{oc}}(n))$ shall be calculated as the final result. The specific calculation formula is as follows:

$$f^*(n) = \begin{cases} H_{\mathrm{oc}}(n), H_{\mathrm{oc}}(n) = H_{\mathrm{co}}(n) \\ H(n), H(n) = H_{\mathrm{co}}(n) \; or \; H(n) = H_{\mathrm{oc}}(n) \\ \mathrm{mean}[H(n), H_{\mathrm{oc}}(n), H_{\mathrm{co}}(n)], \; \mathrm{else} \end{cases} \tag{6}$$

In addition to the combination of theoretical operations, the appropriate selection of structural elements is the key factor to improve the filtering accuracy. The structural elements are mainly composed of three parts: length, height and shape. For noise elimination, the more complex the composition of structural elements,

the better the filtering effect, but it takes a long time. The selection of structural elements is related to the signal waveform and noise types. The common shapes include straight line, semicircle, triangle and curve. A large number of studies have proved that straight line, curve and semicircle have better filtering effect on white noise and triangle has better filtering effect on salt and pepper noise (impulse noise). The length of the structural element depends on the sampling frequency and noise width of the signal to be processed. The length of the structural element should be greater than the noise width and far less than the length of the signal to be processed. If the structural element is too long, the signal will be too smooth and distorted. The height of structural elements should be controlled between 1 and 5% of the main contour of the signal to be processed. In signal processing, it needs to be selected according to the actual situation [18–20].

2.2 EMD

EMD is the key step of HHT algorithm, and the correctness of its result directly determines the correctness of HHT algorithm analysis. EMD can decompose the signal to be processed into a number of intrinsic mode functions (IMF) and obtain the IMF component we need through strict screening. The decomposition process is as follows:

(1) Find out all the local maxima $x_{\max}(t)$ and local minimum $x_{\min}(t)$ of the signal to be processed, connect all the local maxima and local minimum by cubic spline interpolation, form the upper and lower envelope, and calculate the mean $\mathrm{md}_1(t)$;
(2) Subtract the mean $\mathrm{md}_1(t)$ from the original signal to obtain the new signal $x_1(t)$:

$$x_1(t) = x(t) - \mathrm{md}_1(t) \tag{7}$$

Judge $x_1(t)$ according to the judgment basis of IMF component. If $x_1(t)$ does not meet the basis, replace $x_1(t)$ with the original signal and repeat the above steps until $x_1(t)$ meets the judgment basis. At this time, $x_1(t)$ is determined as the first component of IMF and recorded as IMF_1;

(3) Separate $x_1(t)$ from $x(t)$, and repeat steps (1) and (2) with the remaining signal $x(t) - x_1(t)$ as a new signal until $x(t)$ is decomposed to the non-decomposable remaining amount $\mathrm{re}(t)$. At this time, EMD decomposition is completed. At this time, the remaining quantity $\mathrm{re}(t)$ can be expressed by the following formula:

$$\mathrm{r}_e(t) = \frac{\sum_{t=0}^{T} \left|\mathrm{IMF}_{k-1} - \mathrm{IMF}_k\right|^2}{\sum_{t=0}^{T} |\mathrm{IMF}_k|^2} \tag{8}$$

The residual $\mathrm{re}(t)$ is less than 0.1. The original signal can be expressed as:

$$x(t) = \sum_{i=1}^{k} \mathrm{IMF}_i + \mathrm{r}_e(t) \tag{9}$$

In Eq. 9, IMF_i is arranged according to the frequency from high to low.

2.3 Hilbert transform

The EMD method proposed by Huang can be understood as a scale filtering method. After EMD, each IMF component reflects the characteristic scale of the signal and represents the internal modal characteristics of the signal. HHT method can obtain the instantaneous frequency of the IMF component by deriving the IMF component obtained by EMD decomposition. Then, the instantaneous frequencies of all components are accumulated to obtain the Hilbert spectrum of the original signal, which can clearly see the frequency distribution in the signal, to avoid the occurrence of high and low harmonic components in Fourier transform.

Hilbert transform convolutes the original signal with the signal $h(t) = \frac{1}{\pi t}$. Each IMF is taken into the following equation of Hilbert transform.

$$\widehat{x}(t) = h(t) * s(t) = \frac{1}{\pi} \mathrm{PV} \int_{-\infty}^{+\infty} \frac{x(\tau)}{t-\tau} \mathrm{d}\tau \tag{10}$$

where PV represents Cauchy principal value, which can avoid the loss of singularities of individual points and ensure global transformation. This transformation holds for any function in Hilbert space. $x(t)$ and $\widehat{x}(t)$ form complex conjugation and define the analytic signal $z(t)$ about $x(t)$.

$$z(t) = a(t)e^{j\theta(t)} \tag{11}$$

where $a(t) = \sqrt{x^2(t) + \widehat{x}^2(t)}$ is instantaneous amplitude and $\theta(t) = \mathrm{arctg}\frac{\hat{x}(t)}{x(t)}$ is instantaneous phase.

Each IMF has its corresponding instantaneous frequency at different sampling points. The instantaneous frequency can be calculated by deriving the instantaneous phase, and the instantaneous frequency calculation formula is as follows:

$$f_{\mathrm{HZ}}(t) = \frac{\mathrm{d}(\theta(t))}{2\pi\,\mathrm{d}t} = \frac{d\left(\mathrm{arctg}^{\hat{x}(t)}/_{x(t)}\right)}{2\pi\,\mathrm{d}t} \tag{12}$$

The instantaneous amplitude and frequency of each IMF component can be calculated to obtain the corresponding signal component of each IMF, and the original signal can be obtained by superposition, as shown in the following formula:

$$x(t) = \sum_{i=1}^{k} a_i(t)e^{j\theta_i(t)} = \sum_{i=1}^{k} a_i(t)e^{j\int \omega_i(t)\mathrm{d}t} \tag{13}$$

The residual re(t) is either a monotone function or a constant. Although the Hilbert transform can treat the monotonic trend as part of the longer oscillation, the energy involved in the remaining trend may be very strong. Considering the uncertainty of long-term trend and the information contained in other low-energy and high-frequency components, the final non-IMF component should be ignored. Therefore, the remaining amount is omitted in Eq. 13. Since both frequency and amplitude are functions of time, the Hilbert spectrum can be obtained by expanding Eq. 13:

$$P(\omega, t) = \sum_{i=1}^{k} a_i(t) e^{j \frac{1}{2\pi} \int \omega_i(t) \mathrm{d}t} \tag{14}$$

$P(\omega, t)$ is a complete joint spectrum of time, frequency and energy. From it, we can see not only the frequency changes in different time periods, but also the energy changes with the passage of time and frequency. On basis of Hilbert spectrum, Hilbert marginal spectrum is obtained by the following equation:

$$p(\omega) = \int_0^T P(\omega, t) \mathrm{d}t \tag{15}$$

where T represents the total length of signal time series, and Hilbert marginal spectrum represents the amplitude change of different local frequency segments.

2.4 Similarity criterion

The traditional HHT algorithm can obtain the instantaneous frequency of each IMF component through Hilbert transform and then set the low-pass filter with corresponding threshold to filter the IMF component in frequency domain. It has a good effect in reducing white noise, but it will cause signal distortion. To improve the noise processing effect, the similarity criterion is introduced to compare the instantaneous frequency in each IMF components with the frequency distribution range of geomagnetic signal, then, the IMF components are selectively processed, the IMF components with high similarity with the frequency distribution range of geomagnetic signal are retained, the IMF component with low similarity is directly deleted, and the other IMF components are processed by corresponding low-pass filter.

The measured signal of the geomagnetic sensor is a combination of internal noise, external interference and real signal. The IMF components of the measured signal after EMD decomposition are arranged from high to low. The closer the instantaneous frequency of the IMF is to the frequency distribution range of the real signal, the greater the similarity between the two is considered. The geomagnetic signal frequency is composed of geomagnetic reversal frequency and pulsation frequency. The geomagnetic reversal cycle is about 500,000 years, the frequency is close to 0, and the maximum pulsation frequency can reach 5 Hz, so the geomagnetic signal frequency is lower than 5 Hz. To ensure that the real geomagnetic signal frequency can be retained to the greatest extent, the frequency distribution range of the real geomagnetic signal is selected as 0–10 Hz, and the similarity calculation formula is as follows:

$$r_i = \frac{N_{\mathrm{si}}}{N} \tag{16}$$

Table 1 The solution according to similarity r_i

r_i	**Solution**
≥ 0.95	Keep unchanged
≥ 0.05 or $0.95 <$	Low-pass
$0.05 <$	Remove as noise

where r_i is the similarity, and n is the total number of sampling points and is the number of sampling points with instantaneous frequency less than 10 Hz in IMF components. According to the value range of r, the IMF components can be divided into three parts and the corresponding processing methods can be determined, as shown in Table 1:

After the IMF components are judged by similarity criteria, the IMF components are removed as noise, filtered and kept unchanged to obtain a new IMF component. The new IMF component is reconstructed to obtain the processed final signal as follows:

$$x(t) = \sum_{i=1}^{k_1} \mathrm{imf}_i' + \mathrm{r}_e(t) \tag{17}$$

For intuitive view of the chain of IMMF–IHHT algorithm, the overall structure is shown in Fig. 1.

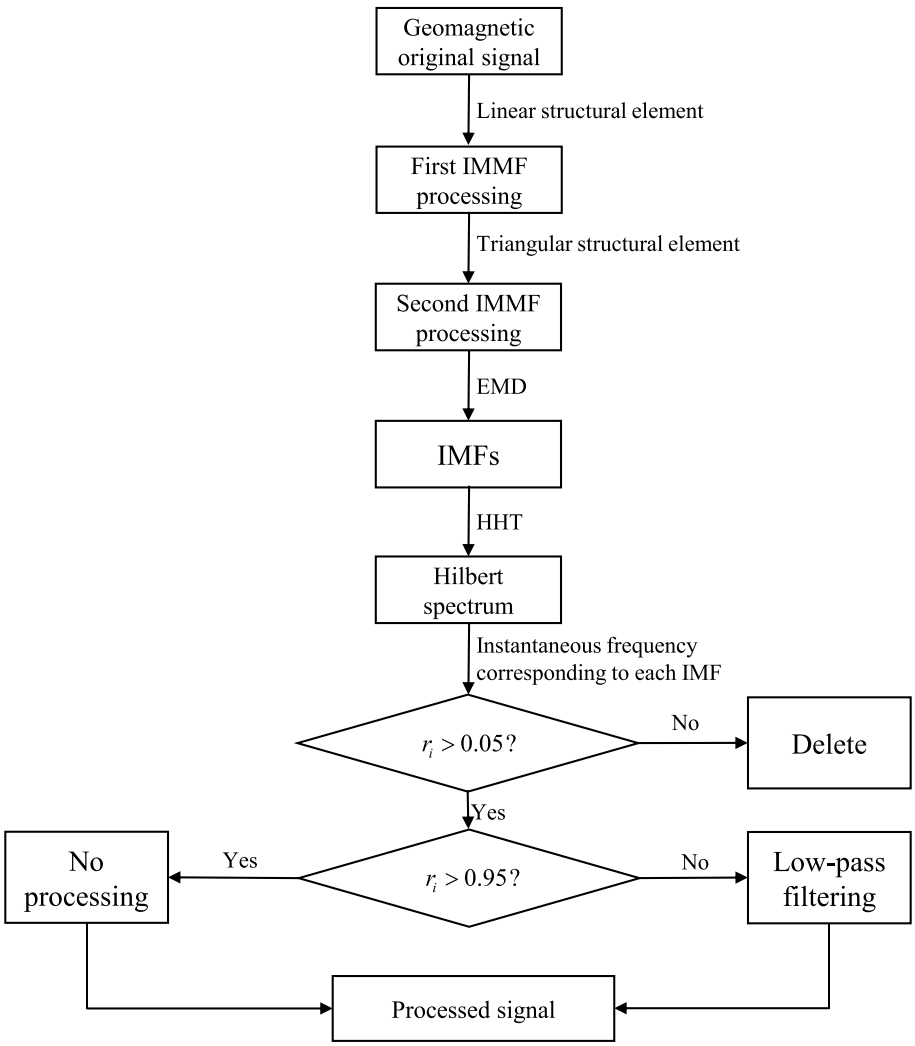

Fig. 1 The overall chain of IMMF–IHHT algorithm

3 Simulation

To verify the superiority of the IMMF for noise processing, the following simulation calculations are carried out. Considering the cosine relationship between the output of geomagnetic sensor and the angle between sensitive axis and geomagnetic component, the signal generation function of the following formula is selected:

$$x(t) = 200\cos(2 * \text{pi} * t) + s(t) \tag{18}$$

where $s(t)$ is the interference signal, including white noise, impulse noise and convex (triangular) noise. The original waveform of the signal is shown in the figure below.

In Fig. 2a, red curve represents the ideal geomagnetic output, and blue curve represents polluted geomagnetic signal. As shown in Fig. 2b, simulated noise contains most common noise in navigation geomagnetic sensor, including white noise, convex noise and impulse noise. The number of sampling points is 1000 times of the sampling time. Triangle, straight line, semicircle and cosine curve structural elements of the same length and height are used to process the original signal, as shown in the figure below. Signal-to-noise ratio (SNR) is introduced to quantify the denoising effect of both. The calculation method is shown in the following formula. The corresponding signal-to-noise ratio is 19.1086, 19.0395, 18.9456 and 18.9652. It can be concluded that the treatment effect of triangular and rectangular structural elements is better (Fig. 3).

$$\text{SNR} = 10\log_{10}\frac{P_{\text{signal}}}{P_{\text{noise}}} \tag{19}$$

In view of the large amount of Gaussian white noise, a small amount of impulse noise and convex noise in the original signal, linear structure elements are selected to process the signal, mainly for the white noise in the original signal. Select the linear structure element $g_{f1} = [1, 1, 1, 1, 1]$, Replace Eq. (6) for processing, and the processed signal is shown in the figure below.

In Fig. 4a, the red curve represents the ideal signal, the blue curve represents the signal after MF processing, and the black curve represents the signal after IMMF processing.

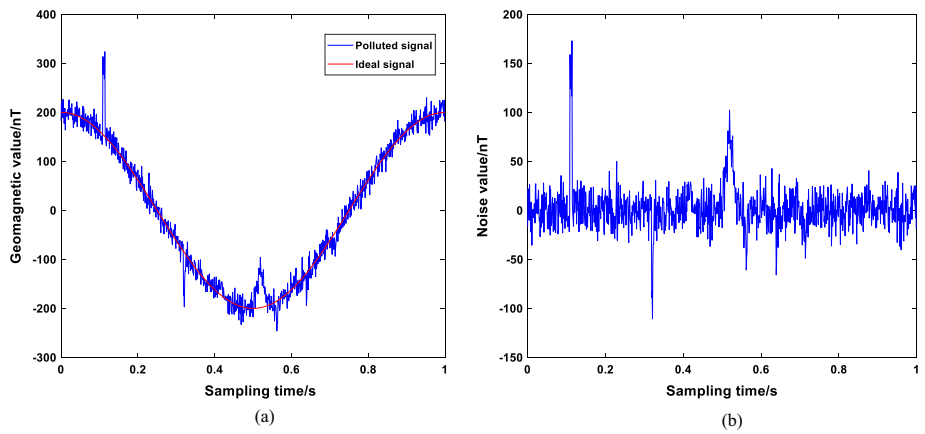

Fig. 2 Polluted geomagnetic signal and ideal signal

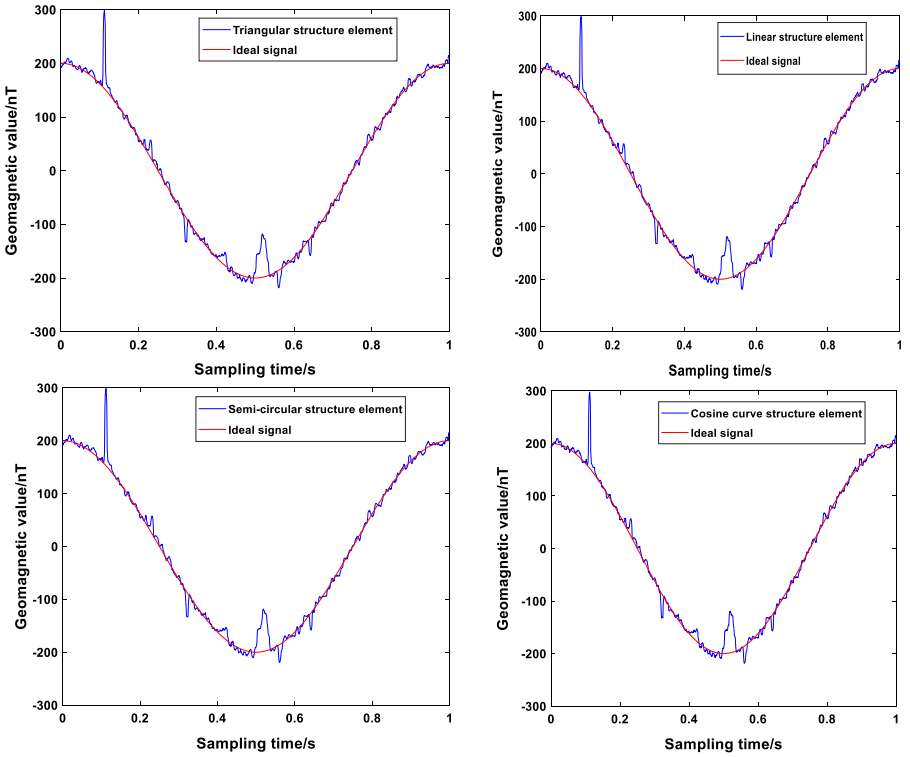

Fig. 3 Comparison of four structural elements

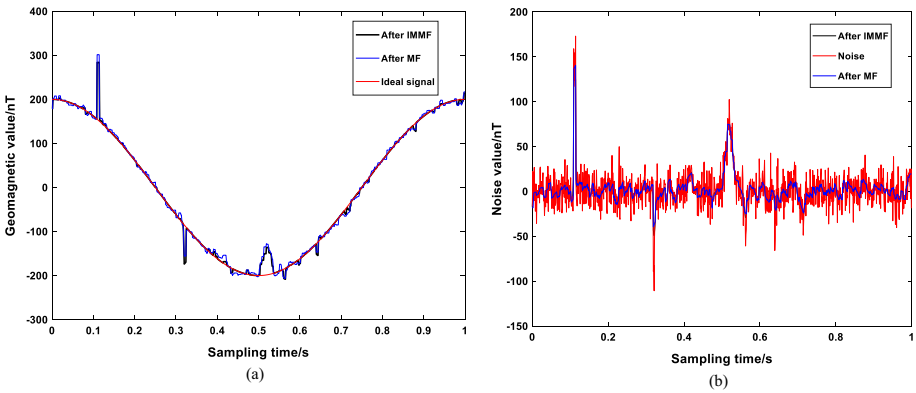

Fig. 4 The ideal signal and processed signal after IMMF and MF

In Fig. 4b, the black curve represents the residual noise after IMMF treatment, the blue curve represents the residual noise after MF treatment, and the red curve represents the noise before treatment. To more clearly compare the denoising ability of IMMF and MF, the SNR is introduced to quantify the denoising effect of IMMF and MF. IMMF and MF are used to process the signal, respectively. The processed signal-to-noise ratio is shown in the table below:

It can be seen from Table 2 that comparison of SNR of geomagnetic measurement signals after the first processing that the SNR of the signal processed by IMMF is greater than that of the signal processed by MF, indicating that the denoising

Table 2 Comparison of SNR of geomagnetic measurement signals after the first processing

Method	SNR (dB)
Original signal	15.8494
MF	18.385
IMMF	19.577

performance of IMMF is better than that of MF. Through comparison, it is obvious that after the IMMF of linear structural elements, the white noise in the interference noise has been greatly improved, and the impulse noise has been partially treated, but the treatment effect has not reached the expectation, and the treatment effect of convex noise is poor. Select the triangular structure element $g_{f2} = [0, 0.01, 0.015, 0.01, 0, -0.01, -0.015, -0.01, 0]$, and the signal after the second IMMF processing is shown in the figure below.

The meaning of curve color in Fig. 5 is the same as that in Fig. 4. The geomagnetic measurement signal processed by IMMF and MF of triangular structural elements is brought into Eq. 19, and their SNR is calculated to obtain the following table.

It can be seen from Table 3 that the SNR of IMMF of triangular structural elements is greater than MF, indicating that the denoising performance of IMMF is better than MF. In Fig. 5, the Gaussian white noise and impulse noise are basically eliminated, the convex noise is not significantly improved, and the noise amplitude of other sampling points is reduced from ± 50 to ± 20nt. To further verify that the high-frequency noise is basically eliminated and compare it in the frequency domain, this paper performs Hilbert transform on the signals before and after IMMF processing to obtain the corresponding Hilbert spectrum, as shown in the figure below.

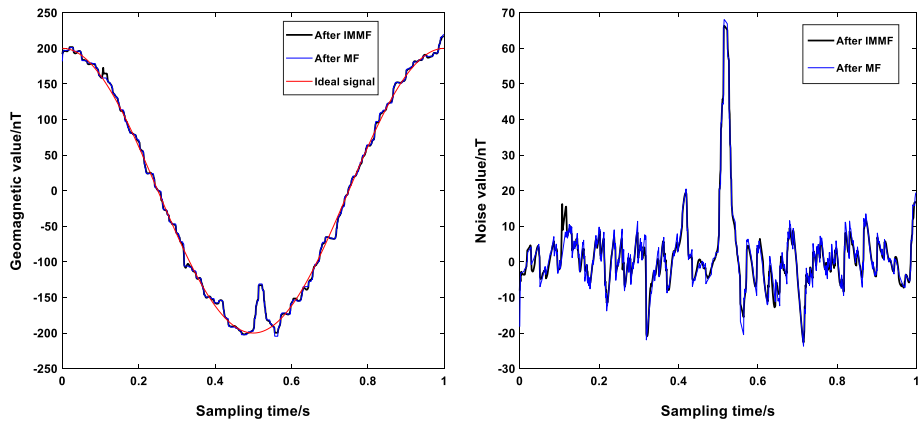

Fig. 5 The ideal signal and processed signal after second IMMF and MF based on triangle structure element

Table 3 Comparison of SNR of geomagnetic measurement signals after the second processing

Method	SNR (dB)
MF	22.1447
IMMF	22.3317

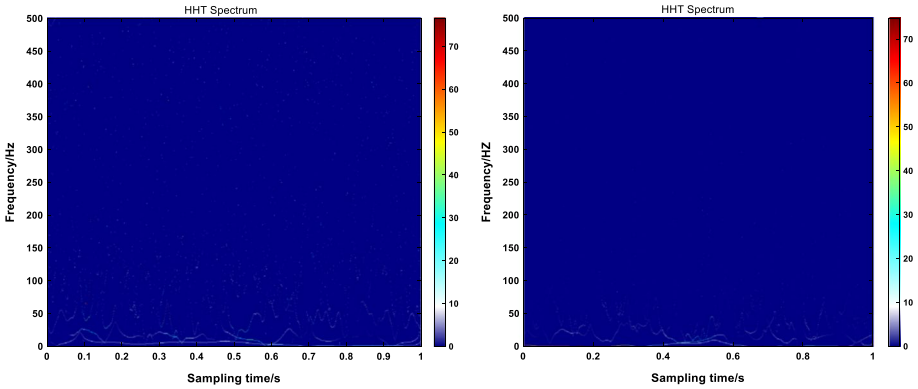

Fig. 6 HHT spectrum of signals before and after IMMF processing

In Fig. 6, the horizontal ordinate represents the sampling time, the vertical ordinate represents the signal frequency, and the color point represents the signal amplitude. Figure 6a shows the HHT spectrum of the original signal not processed by IMMF, and Fig. 6b shows the HHT spectrum of the signal processed by IMMF. In Fig. 6a, the color points are widely distributed and scattered, and there are many high-frequency noises. After two IMMF processing, the signal frequency distribution is shown in Fig. 6b, the high-frequency noise is basically eliminated, and the color points are mainly concentrated below 100 Hz. To further eliminate the noise in the signal and improve the signal-to-noise ratio of the signal, EMD is performed on the signal after two IMMF processing, and five IMF components and residuals are obtained, as shown in the figure below (Fig. 7).

Figure 8 shows a partial enlarged view of Fig. 6b. In Fig. 7, the corresponding ordinate of the red line is 1 Hz, which can be considered as the ideal signal frequency. Set the similar frequency range below 2 Hz, compare the instantaneous frequency of each IMF component, and get the similarity between the instantaneous frequency of IMF component and ideal signal, as shown in the table below:

It can be seen from Table 4 that IMF1–IMF3 components are not similar to ideal signals and can be directly removed as noise signals. The IMF4 component is similar to the ideal signal part and needs low-pass filtering. Set the threshold frequency of the filter to 2 Hz. The IMF5 component is highly similar to the ideal signal and does not require any processing. After the IMF component is processed, the reconstructed signal is obtained according to Eq. 17, that is, the processed final signal, as shown in the figure below.

Figure 9a shows a comparison between the final processed signal and the ideal signal. The red curve represents the ideal signal, and the blue curve represents the signal after the final processing. Figure 9b shows residual noise after final processing. As can be seen from Fig. 9, the noise intensity is reduced to −3–18nT after IMMF–IHHT treatment, and the convex noise, Gaussian white noise and impulse noise are basically removed. To show the superiority of IMMF–IHHT combined filtering algorithm in denoising, we reproduce the algorithms of Li Ji and Zhou (Li Ji's algorithm is MF-HHT and Zhou's algorithm is IHHT, see (a) and (b) below, respectively), process the same original signal,

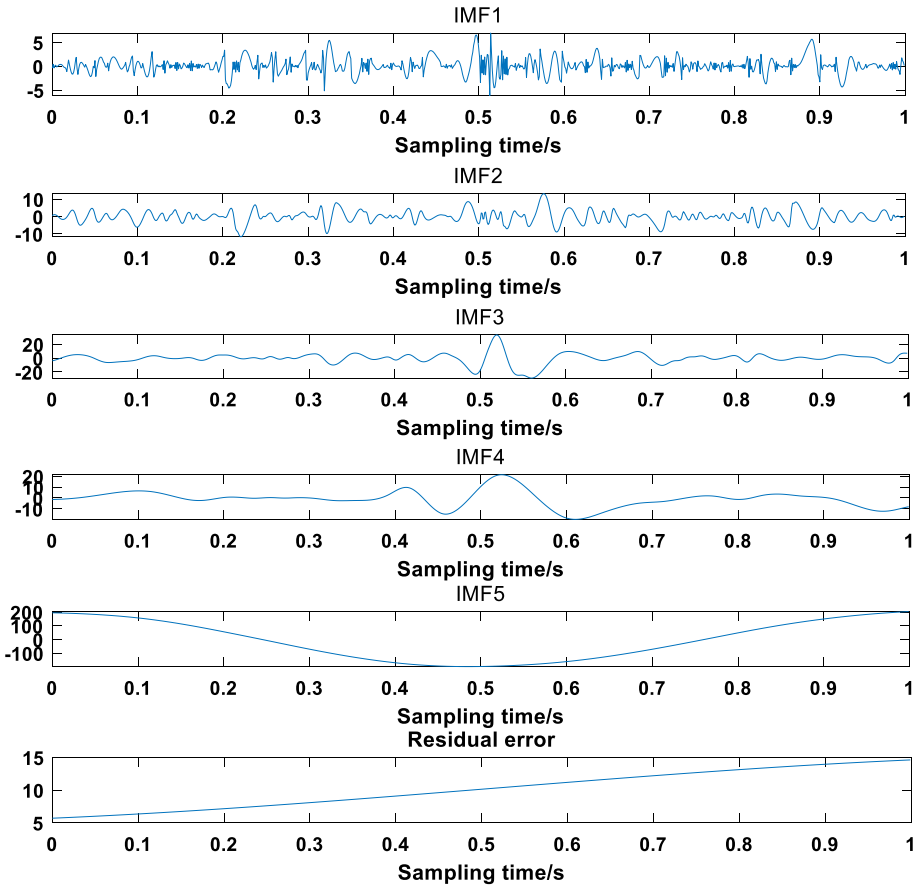

Fig. 7 EMD (five IMFs and residual)

and compare the final results. The processing results of Li Ji' algorithm and Zhou's algorithm are shown in Figs. 10, 11 and 12.

To quantify the processing effect, the residual noise range and SNR are used to evaluate the denoising effect of the three processing methods, as shown in the table below.

It can be seen from Table 5 that the range and signal-to-noise ratio of signal residual noise processed by IMMF–IHHT combined filtering algorithm are better than the other two algorithms, which shows that the denoising performance of IMMF–IHHT algorithm is better than the other two algorithms.

4 Experimental investigation

To discuss the effect of using IMMF–IHHT algorithm in practical application, we install the sensor on the vibration turntable. The vibration turntable is to simulate the vibration of the carrier in the movement process, observe the output signal of the geomagnetic sensor in the vibration state, and verify whether the filtering can effectively eliminate the influence of vibration on the sensor output. The geomagnetic sensor signal measurement system is composed of sensor (HMC1053), main control board and SPI serial port line. The geomagnetic sensor chip is HMC1053 chip of Honeywell company of the USA. The data collected by the sensor are transmitted to the main control board and then

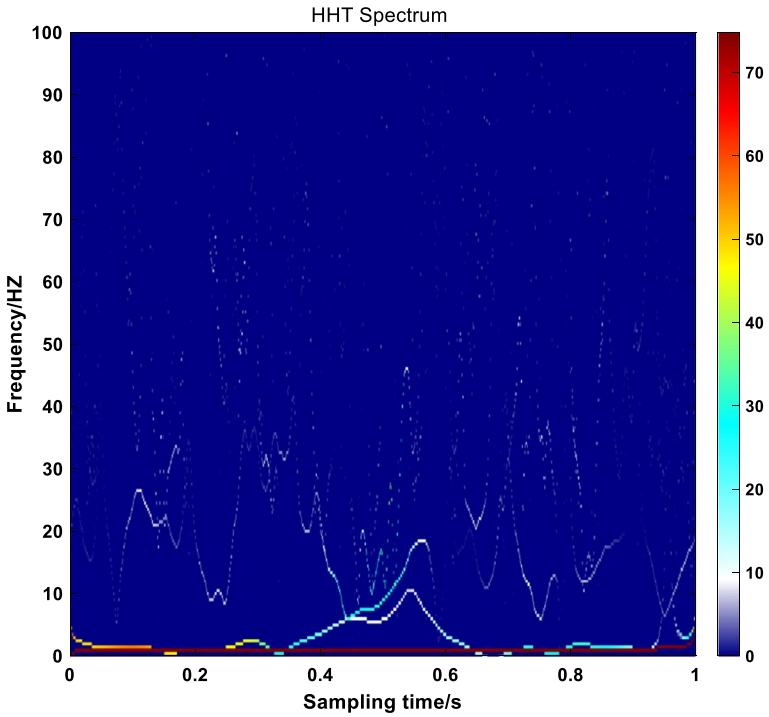

Fig. 8 HHT spectrum local amplification

Table 4 Similarity between ideal signal and IMF components

	IMF1	IMF2	IMF3	IMF4	IMF5
r_i	0	0	0.003	0.0832	0.998

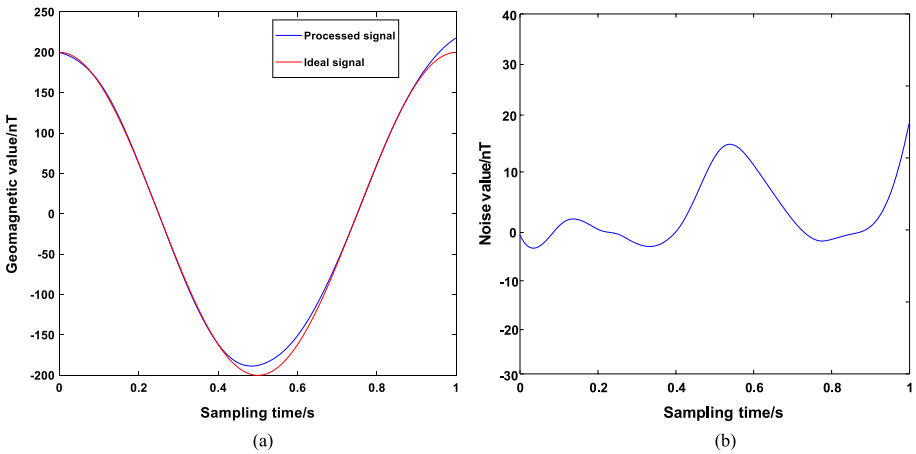

Fig. 9 Final processed signal and ideal signal

transmitted to the upper computer by the main control board through SPI serial port line. The experimental environment is shown in Fig. 13. We choose to place the experimental equipment on the wooden table in the open space and use the level instrument

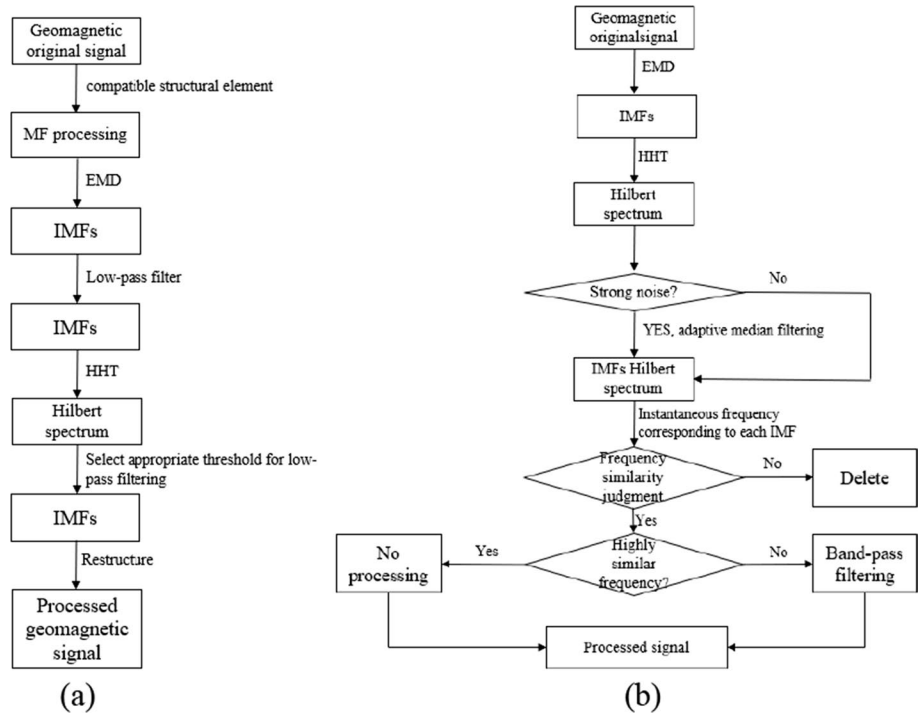

Fig. 10 **a** is Li Ji's algorithm and **b** is Zhou's algorithm

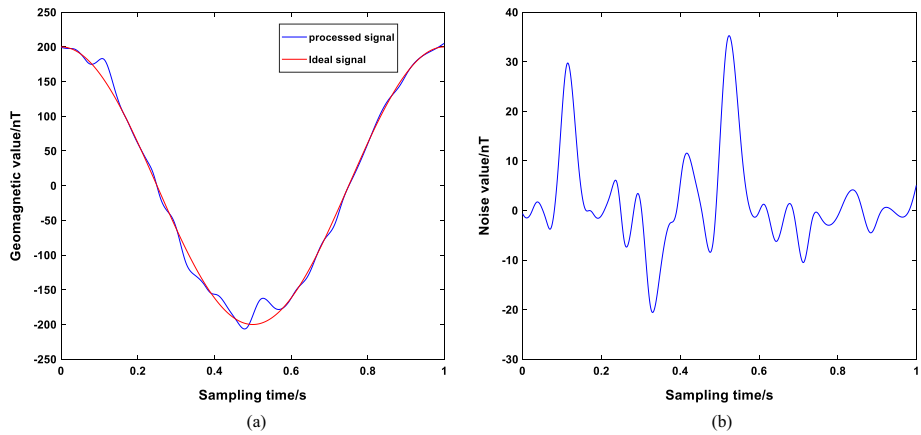

Fig. 11 Signal processing results of Li Ji's algorithm

(with an accuracy of 0.02 mm/m) to adjust the table to the horizontal state. The shell of the vibration turntable is composed of superhard aluminum alloy, and its vibration function is completed by the servo motor. The operation of the motor is transmitted by the controller. Measured by FM3000 magnetic field detector, the servo motor has little impact on the geomagnetic field on the surface of the turntable, so the motor can be regarded as only bringing noise interference to the sensor during operation.

The turntable is controlled in one direction (away from the blind area of geomagnetic measurement), and the controller sends the cosine command with vibration frequency of 20 HZ and amplitude of 0.5 cm to the turntable to collect the three-axis output data of

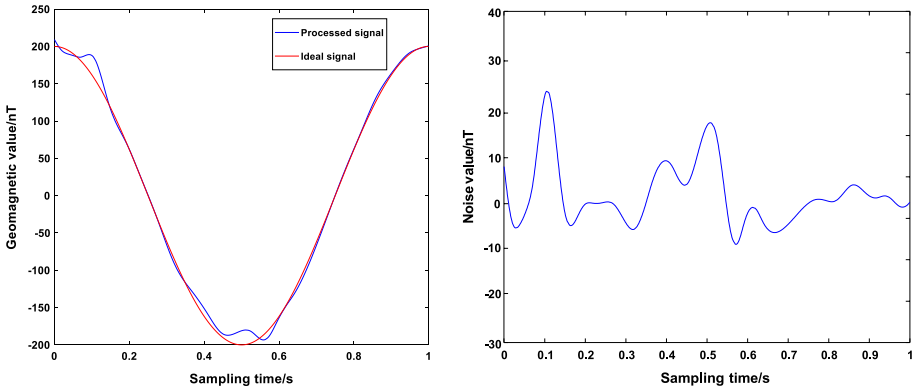

(a) (b)

Fig. 12 Signal processing results of Zhou's algorithm

Table 5 Residual noise range and SNR of three algorithm

Algorithm	Li Ji's algorithm	Zhou's algorithm	IMMF–IHHT
Residual noise (nT)	[− 22, 36]	[− 10, 27]	[− 3, 18]
SNR(dB)	23.5803	25.2552	27.3520

Fig. 13 Experimental environment

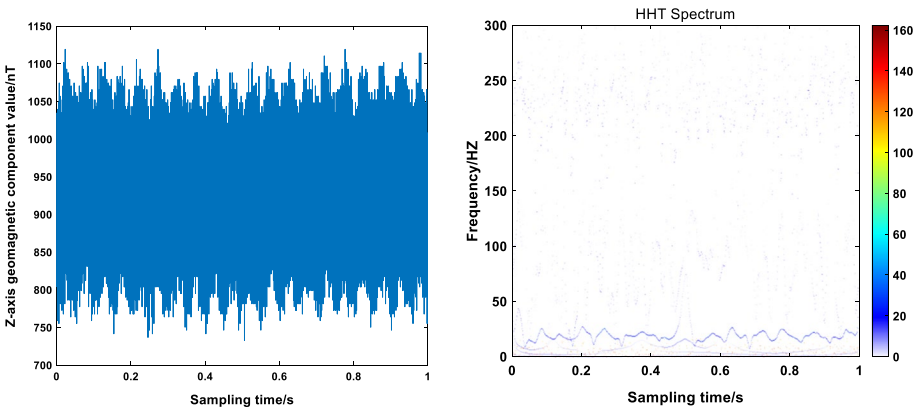

(a) (b)

Fig. 14 H_Z and HHT spectrum of original measurement signal of geomagnetic sensor Z-axis

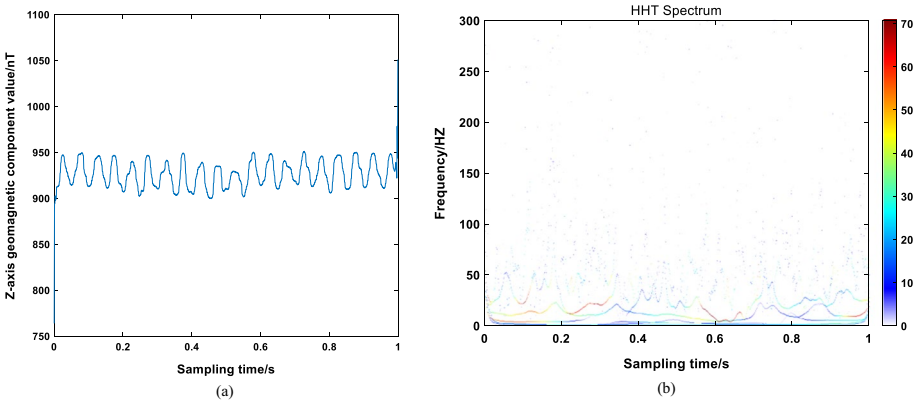

Fig. 15 Geomagnetic measurement signal and HHT spectrum after two IMMF processing

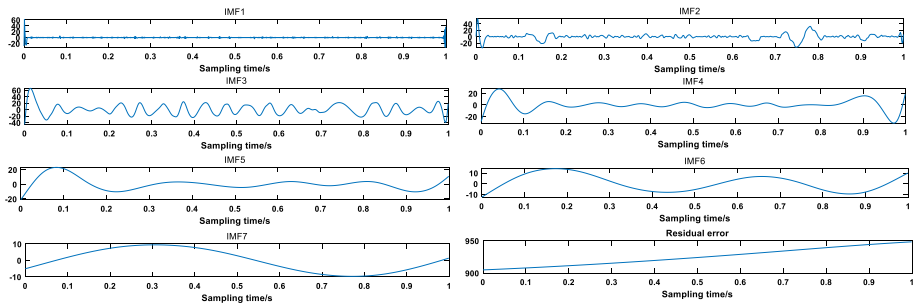

Fig. 16 EMD (seven IMFs and residual)

geomagnetic sensor. Considering that the output signals of the three axes of the sensor have the same characteristics, we take the Z-axis output data H_Z as an example for filtering. Firstly, the time domain diagram and Hilbert spectrum of Z-axis output signal are calculated and drawn, as shown in Fig. 14.

In the HHT spectrum, the abscissa represents the sampling time, the longitudinal ordinate represents the signal frequency, and the color point represents the signal amplitude. The signal amplitude is widely distributed, and IMMF is used to preprocess the original signal. Select linear structural elements [1, 1, 1, 1, 1] and triangular structural elements [0, 0.05, 0.1, 0.05, 0, −0.05, −0.1, −0.05, 0] to process the original signal. The time domain diagram and HHT spectrum of the processed signal are shown in Fig. 15.

It can be seen from Fig. 15 that the high-frequency noise is effectively removed after the geomagnetic measurement signal is processed by two IMMF. EMD is performed on the geomagnetic measurement signal processed by two IMMF, as shown in Fig. 16. IMF components are arranged from high frequency to low frequency, in which IMF1 has the highest frequency and IMF7 has the lowest frequency. The frequency distribution of IMF component determines the accuracy of similarity calculation criterion. The premise of similarity criterion is to know the geomagnetic signal frequency and IMF frequency distribution. The geomagnetic signal frequency is lower than 5HZ, and 10HZ is selected as the cutoff frequency. The instantaneous frequency points of IMF1, IMF2, IMF3 and IMF4 lower than 10 Hz account for 0.0342, 0.0321, 0.0431 and 0.6914, respectively. IMF4 needs low-pass filtering with a cutoff frequency of 10 Hz. To visually observe the

instantaneous frequency distribution of IMF1–IMF4, HHT spectrum is made, respectively. As shown in Fig. 14, the frequency distribution from IMF1 to IMF4 is more and more concentrated, and the frequency of IMF1 is scattered in the whole figure. The frequency of IMF3 is mainly concentrated near 20HZ, which is the vibration signal of turntable, while the frequency of IMF4 is relatively concentrated in the low-frequency region. The instantaneous frequency points of IMF5, IMF6 and IMF7 lower than 10 Hz account for 0.978, 0.976 and 0.994, respectively, which need not be processed.

After the IMF components is processed, the signal is reconstructed according to Eq. 17, and the comparison diagram between the two IMMF and the reconstructed signal is obtained as shown in Fig. 17.

In Fig. 18, the red curve represents the geomagnetic signal after IMMF–IHHT processing, and the blue curve represents the geomagnetic signal after twice IMMF processing. As can be seen from Fig. 18, the noise of the z-axis signal after IMMF–IHHT processing is basically eliminated. According to the processing method of Z-axis geomagnetic signal, the X-axis and Y-axis output signals H_X and H_Y of geomagnetic sensor are processed, respectively, and finally the total intensity H_t of geomagnetic signal is calculated. By measuring the longitude (38° 3′ N), latitude (114° 29′ E) and altitude of 107 m of the experimental site, and using the latest International Geomagnetic Reference Field

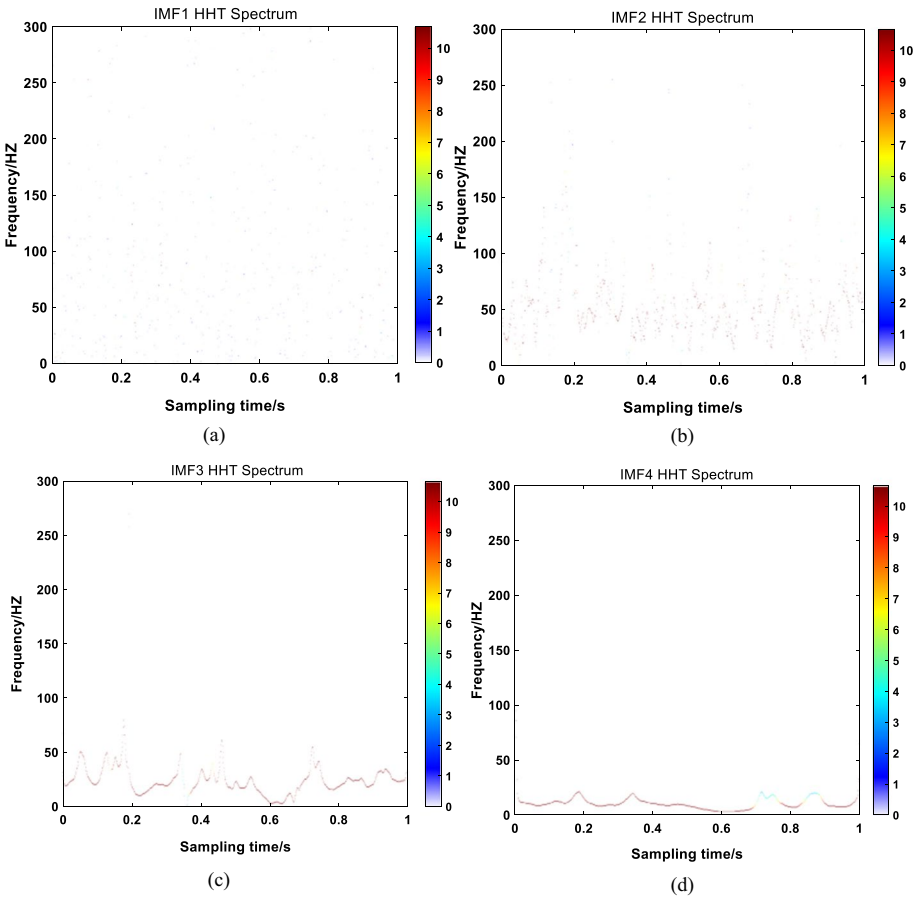

Fig. 17 IMF1–IMF4 HHT spectrum

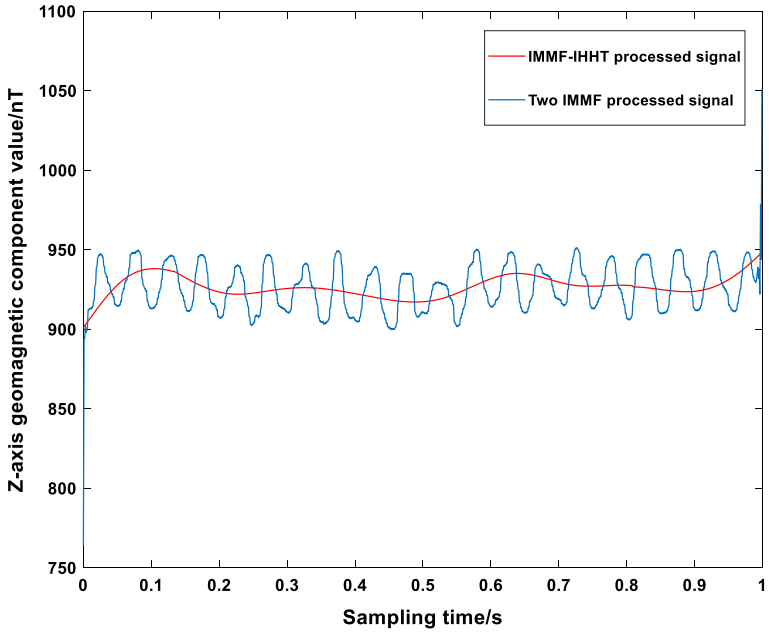

Fig. 18 Comparison between IMMF–IHHT processed signal and two IMMF processed signals

(IGRF) given by the International Association of Geomagnetism and Aerology (IAGA), the magnetic inclination of the geomagnetic field is $-57.3°$. (It is specified that it is positive upward.) The magnetic declination angle is 6.4° (it is specified that the north by west is positive), and the geomagnetic field intensity is 54207 nT. To verify the effectiveness and superiority of IMMF–IHHT in denoising, we reproduce Li Ji's algorithm and Zhou's algorithm, respectively, and compare them with IMMF–IHHT combination algorithm, as shown in the figure below.

In Fig. 19, the blue curve represents Li Ji's algorithm, the red curve represents Zhou's algorithm, the green curve represents IMMF–IHHT combined filtering algorithm, and the black curve represents the reference value of geomagnetic intensity. It can be seen from Fig. 19 that the closer to the black curve, the higher the geomagnetic measurement accuracy. To more intuitively compare the accuracy of the three algorithms, the root-mean-square error (RMSE) is introduced to compare the three algorithms. Their root-mean-square error values are shown in the table below (Table 6).

Through comparison, it is found that the RMSE of IMMF–IHHT is the smallest among the three algorithms, which shows that the filtering effect of IMMF–IHHT for geomagnetic measurement signal is the best.

5 Discussion

5.1 Experimental environment

Choosing an open site can avoid the influence of ferromagnetic materials such as buildings on geomagnetic field measurement. Using the turntable whose shell is made of non-magnetic material can avoid the eddy current magnetic field and induced magnetic field generated by the turntable under the condition of power on vibration, which will affect the geomagnetic field measurement. Keeping the desktop level, the blind area range of

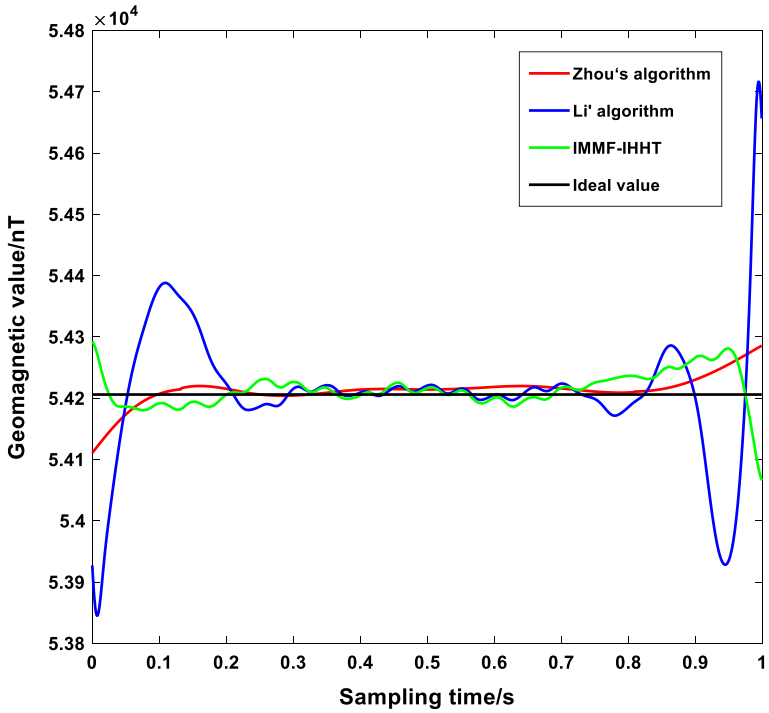

Fig. 19 Comparison of denoising effects of three algorithms

Table 6 RMSE of three algorithm

Algorithm	RMSE
Zhou's algorithm	29.08
Li's algorithm	106.43
IMMF–IHHT	23.96

geomagnetic measurement can be calculated to keep the sensitive axis of the sensor away from the influence of the blind area. By measuring the magnetic field change of the turntable shell with FM3000 magnetometer, it is found that the eddy current magnetic field and induced magnetic field generated by the motor inside the turntable have little influence on the external magnetic field of the turntable when the turntable is powered ON or OFF. In geomagnetic navigation, the vibration accompanying the movement of the navigation carrier will seriously interfere with the measurement accuracy of the geomagnetic sensor and make the turntable vibrate continuously in order to simulate the carrier vibration with high fidelity. In this case, the background contains various random errors and vibration interference, which is suitable for algorithm verification.

5.2 Using mean to improve morphological filtering

In the process of MF algorithm, the shrinkage of open operation leads to the small output of open–close filter, and the expansion of closed operation leads to the small output of close–open filter. The traditional MF uses the average value of the open–close filter and the close–open filter to overcome the defects of the open–close filter and the close–open filter.

The small amount of the open–close filter and the large amount of the close–open filter change with the different signals. In this paper, a segment of signal with the same length as the structure element is selected, and the mean value of this segment of signal is calculated to constrain the results of the open–close filter and the close–open filter, forming the structure of IMMF algorithm. Simulation results show that the denoising performance of IMMF algorithm proposed in this paper is better than MF.

5.3 The IMF components is selectively processed by using the similarity criterion

In fact, the thresholds of the three groups (i.e., 5% and 95%) are designed by referring to the threshold of cosine similarity and the frequency distribution range of the real geomagnetic signal, which can achieve no loss of the real signal frequency and effective suppression of noise. Since the frequency distribution law of geomagnetic signal is not easy to determine, set the upper limit of geomagnetic signal frequency to 10 Hz, calculate the instantaneous frequency of each IMF component at each sampling point, so as to calculate the proportion of sampling points whose instantaneous frequency of IMF component is lower than 10 Hz in the total sampling points, and determine the processing method of IMF component. In this study, we focus on method improvement, so it is possible to carry out improvement work in the future.

6 Conclusion

In geomagnetic navigation, the vibration of the carrier in the process of movement will seriously interfere with the measurement signal of the sensor, so it is necessary to use the denoising algorithm to process the noise. In this paper, a combined algorithm based on IMMF–IHHT algorithm is proposed to suppress the influence of vibration and electromagnetic interference on the sensor. Using IMMF algorithm to preprocess the measurement signal of the sensor and eliminate the pulse high-frequency signal in the signal can effectively avoid the spectrum aliasing in the subsequent EMD decomposition and then improve the quality in the decomposition process. By calculating the proportion of each IMF component in the frequency range of geomagnetic signal and selecting the corresponding processing method of IMF component, we can ensure that the real geomagnetic signal is not lost to the greatest extent. Through simulation and experiments, the superiority of IMMF–IHHT combined algorithm in geomagnetic signal denoising is verified.

Acknowledgements
The authors are not grateful for the financial support.

Availability of data and materials
Please contact author for data requests.

Declarations

Competing interests
The authors declare that they have no known competing financial interests or personal relationships that could have appeared to influence the work reported in this paper.

Received: 31 August 2022 Accepted: 26 January 2023
Published online: 08 February 2023

References

1. Q.Z. Li, Z.N. Li, Y.T. Zhang et al., Integrated compensation and rotation alignment for three-axis magnetic sensors array. IEEE Trans. Magn. **54**(10), 1–11 (2018)
2. W.S. Zeng, Q. Bian, J.J. Gao et al., Attitude-independent magnetometer calibration based on adaptive filtering. IEEE Sens. J. **22**(1), 195–202 (2022)
3. J. Keighobadi, Fuzzy calibration of a magnetic compass for vehicular applications. Mech. Syst. Signal Process **25**(6), 1973–1987 (2011)
4. N.E. Huang, Z. Shen, S.R. Long et al., The empirical mode decomposition and the Hilbert spectrum for nonlinear and non-stationary time series analysis. Proc. R. Soc. Math. Phys. Eng. Sci. **1998**(454), 903–995 (1971)
5. N. Qiao, L.H. Wang, Q.Y. Liu et al., Multi-scale eigenvalues empirical mode decomposition for geomagnetic signal filtering. Measurement **146**, 885–891 (2019)
6. Y. Zhou, X. Zhang, W. Xiao, Calibration and compensation method of three-axis geomagnetic sensor based on pre-processing total least square iteration. J. Instrum. **13**(4), T04006 (2018)
7. C. Xiang, X.Z. Bu, B. Yang, Three different attitude measurements of spinning projectile based on magnetic sensors. Measurement **47**, 331–340 (2014)
8. J. Serra, Morphological filtering-an overview. Signal Process **38**(1), 3–11 (1994)
9. M.J. Shi, M.F. Zhang, L. Gu et al., Research on denoising method of metal magnetic memory signal. J. Magn. **25**(4), 556–566 (2020)
10. M.J. Shi, Y.B. Liang, M.F. Zhang et al., Pipeline damage detection based on metal magnetic memory. IEEE Trans. Magn. **57**(8), 1–5 (2021)
11. Z.C. Shan, J.X. Zhou, J.Y. Chen, et al. Background noise suppression of magnetic anomaly signal based on wavelet transform. in *Proceedings of the IEEE 17th International Conference on Communication Technology (ICCT)*. (Chengdu, 2017).
12. F. Xie, Y. Teng, X. Hu, Application of mathematical morphology-based filter in denoising geomagnetic data. Prog. Geophys. **26**(1), 147–156 (2011)
13. N.E. Huang, Z.H. Wu. A review on Hilbert–Huang transform: method and its applications to geophysical studies. Rev. Geophys. 2008;46(2).
14. J. Li, M. Pan, Y. Tang et al., Analysis and preprocessing of geomagnetic signals based on morphological filter and Hilbert–Huang transform. Chin. J. Sci. Instrum. **33**(10), 2175–2180 (2012)
15. Y. Diao, J. Gao, G. Wu et al., Analysis and preprocessing of STCM signals based on morphology-HHT algorithm. J. Mar. Sci. **39**(3), 44–52 (2021)
16. H.Q. Zhai, L.H. Wang, Q.Y. Liu et al., Geomagnetic signal de-noising method based on improved empirical mode decomposition and morphological filtering. Proc. Inst. Mech. Eng. Part G J. Aerosp. Eng. **235**(5), 578–588 (2021)
17. Y.K. Zhou, G. Huang, X.Y. Zhang, Geomagnetic sensor noise reduction for improving calibration compensation accuracy based on improved HHT algorithm. IEEE Sens. J. **19**(24), 12096–12104 (2019)
18. N. Yu, H. Wu, C.Y. Wu et al., Automatic target detection by optimal morphological filters. J. Comput. Sci. Technol. **18**(1), 29–40 (2003)
19. A.J. Hu, L. Xiang, Selection principle of mathematical morphological operators in vibration signal processing. J. Vib. Control **22**(14), 3157–3168 (2016)
20. Z. Wen-Bin, Y. Chen-Long, Z. Xiao-Jun, Application of morphology filtering method in vibration signal de-noising. J. Zhejiang Univ. Eng. Sci. **43**(11), 2096–2099 (2009)

Publisher's Note